

Divergent short- and long-range behavior in ion-irradiated δ -Sc₄Hf₃O₁₂Maulik K. Patel **Department of Mechanical, Materials, and Aerospace Engineering, University of Liverpool, Liverpool L69 3GH, United Kingdom*Kurt E. Sickafus[†]*Department of Materials Science and Engineering, University of Tennessee, Knoxville, Tennessee 37996, USA*Gianguido Baldinozzi ‡*Structures, Propriétés, et Modélisation des Solides, Université Paris-Saclay, CentraleSupélec, CNRS, 91190 Gif-sur-Yvette, France*

(Received 12 June 2020; accepted 14 August 2020; published 15 September 2020)

Ion irradiation experiments and quantitative x-ray diffraction analysis were used to demonstrate that the lattice and structure behave very differently in a complex oxide, δ -Sc₄Hf₃O₁₂, under irradiation. Analysis of the structure reveals that with increasing fluence, the characteristic c/a ratio for the δ phase converges to that of an ideal fluorite phase, whereas locally it produces a metaphase consisting of frozen nanoscale structures having bixbyite-like fluorite that increase the overall stability and radiation response of the apparent long-range oxygen-deficient average fluorite structure.

DOI: [10.1103/PhysRevMaterials.4.093605](https://doi.org/10.1103/PhysRevMaterials.4.093605)

I. INTRODUCTION

Nonstoichiometric fluorite-related oxides are model systems to address fundamental questions in inorganic compounds, and in particular the mechanisms of solid state reactions and transformations in solids. Systematic analysis of the thermodynamic properties of heterogeneous equilibria shows that singularities of the physical properties (melting point, conductivity, thermoelectricity, etc.) do not necessarily occur for compositions with simple rational ratios. Wagner and Schottky [1] discussed the statistical thermodynamics of real compounds and proved the stoichiometry of ideal crystals has no special position, though the extent to which different substances may display a departure from stoichiometry depends on specific characteristics like the energies of lattice disorder and charge transfer. Oxygen-deficient fluorites are grossly nonstoichiometric compounds and lattice energy calculations can lead to the conclusion that many of the observed nonstoichiometric phases can exhibit a high degree of metastability [2]. Indeed, in these systems, short-range interactions between defects, clusters, and complex atomic arrangements can be strong and they can explain the observed variety of long-range structures encountered in these compounds. The delicate balance between order, disorder, and metastability present in these systems makes them an interesting playground for studying their resilience to external perturbations, and in particular, to ion irradiation. Though the questions raised are fundamental, their impact on properties is also important. Structural stability is of particular interest in

these complex oxides because these systems provide fascinating insights into the behavior of advanced nuclear ceramics and the long-term behavior of spent fuels and nuclear waste forms. The technological interest in these oxides also spans other areas as they find applications as solid state electrolytes in fuel cells, and have interesting features that can be exploited in the engineering of thermal barrier coatings.

As the structures disorder, they become more complicated and difficult to describe. But disorder and complexity by themselves are neither good nor bad. It is the lack of precision in their description that often prevents us from navigating and managing this complexity. A complete description of all the phenomena occurring in fluorite-related materials disordered by ion irradiation is still out of reach.

The study of radiation effects in fluorite compounds and in fluorite derivative phases, including pyrochlore, weberite, and bixbyite systems, is not a recent trend, though it is still expanding. Pyrochlores and weberites [3] with $A_2B_2O_7$ generic chemical formula are perhaps the simplest and least substoichiometric compounds in the AO_{2-x} system where there is a significant tendency for cations and anions to order. Several studies highlight the impact of the A - and B -site cation radii on the resistance to disorder or amorphization produced by high pressure or radiation [4–10]. Bixbyite oxides (B_2O_3) generally consist of a single type of rare-earth cation. These systems exhibit a consistent ordering of O vacancies in their ground state. Moreover, these structures display the highest oxygen deficiency among the fluorite-related systems. While recent structural studies using diffraction techniques assess the structural changes occurring in these single-element oxides [11–13], little is structurally known about multication bixbyites [14,15].

In between these two substoichiometric compositions of the oxygen-deficient fluorite systems, another simple system

*maulik.patel@liverpool.ac.uk

†kurt@utk.edu

‡gianguido.baldinozzi@centralesupelec.fr

that exhibits a consistent anion vacancy ordering, not necessarily involving cation ordering, is the δ -phase structure. The radiation resistance of these structures has already been investigated using diffraction techniques but the details of the structural changes are not yet clear as there is no extensive and systematic study of these systems using x-ray or neutron diffraction. δ phases are interesting systems in the large family of oxygen-deficient fluorites [16]. The δ -phase structure consists of edge- and corner-sharing oxygen octahedra and oxygen vacancies are located in the ideal fluorite anion sublattice. These vacancies are generally found to order onto specific sites of the structure, leading to the appearance of superstructure reflections in the x-ray diffraction patterns. These weak reflections are produced by the combined effect of the composition modulation and of the displacive relaxation of the metal ions surrounding the anion vacant sites. The ideal oxygen stoichiometry (O/M) in δ phases is close to 1.714. Direct structural determination has found that the cations order only when the stoichiometry is $A_6^{+3}B^{+6}O_{12}$ [17,18], whereas the cations cannot order in compounds with stoichiometry $A_4^{+3}B_3^{+4}O_{12}$. The common characteristic symmetry of these phases is $R\bar{3}$, and they typically exhibit a moderate deviation (a few %) from the ideal c/a ratio 0.9258 of a cubic fluorite described in this same lattice frame.

The structural characteristics of several irradiated δ phases [19–26] were studied and the common conclusion was the observation of a phase transformation toward an apparent disordered fluorite phase. The most comprehensive among these studies [20,21] also discuss the qualitative formation of a bixbyite-like phase in low-energy irradiated δ - $\text{Sc}_4\text{Zr}_3\text{O}_{12}$. This transformation to bixbyite was in some ways a mystery since group-subgroup analysis does not allow for a direct transformation from the δ phase to a bixbyite. However, if one compares the polyhedral networks in these two structures, then one can find a slight similarity in the polyhedral networks. The bixbyite structure is only composed of octahedra (slightly distorted octahedra [27]), while the δ phase is typically described as having 6-fold and 7-fold polyhedra. However, one of the M - O bond lengths in the 7-fold polyhedra is significantly longer such that the polyhedra resemble capped octahedra [28].

The aim of this work is not to provide a definitive blueprint for the global changes occurring in all fluorite-derived structures, but rather to offer a fresh explanation for the following phenomena: (1) the critical structural changes involved; (2) how structure supports radiation resistance; (3) how to find a balance between global long-range and diverse local structural features; and (4) how this can lead to effective engineering of fluorite-related materials. In order to establish these quantitative features, we analyze structural characteristics of a swift heavy ion irradiated δ -phase compound, namely $\text{Sc}_4^{+3}\text{Hf}_3^{+4}\text{O}_{12}$, using high-resolution x-ray powder diffraction.

II. EXPERIMENTAL PROCEDURES

Powders of scandium sesquioxide (Sc_2O_3 , 99.99%) and hafnium oxide (HfO_2 , 99.95%) purchased from Alfa Aesar were calcined at 700 °C and weighed to obtain a 4:3:12 stoichiometric ratio of Sc:Hf:O. The mixture was ball milled in a

high-energy SPEX 8000D dual mixer/mill using a zirconia ceramic vial set and two 12.7 mm zirconia ceramic balls in an isopropanol medium for 8 hours. The powder mixture was cold pressed into pellets of 13 mm in diameter and a thickness of 10 mm using a stainless steel die and plunger. The pellets were then sintered in air, first at 1200 °C for 48 hours and then again at 1600 °C for 72 hours. The heating and cooling rates during both sintering cycles were kept at 5 °C/min. Samples were ground again between the two sintering cycles. The as-synthesized pellets were close to 95% of the theoretical density and x-ray powder diffraction was performed to assess their phase purity. Qualitative analysis of the diffraction patterns showed formation of a rhombohedral δ phase that matched closely with structures reported in the literature [16,29].

The rest of the pellets were used for irradiation experiments. Prior to irradiations, these pellets were cut into disks of 2 mm thickness and polished with diamond lapping films down to 1 μm . The final polishing was performed using colloidal silica to remove residual damage due to polishing. To study the radiation response of δ - $\text{Sc}_4\text{Hf}_3\text{O}_{12}$, samples were irradiated at room temperature with 92 MeV Xe^{26+} ions at the IRRSUD beamline in GANIL, France, using time-integrated fluxes (fluences) ranging from 10^{11} to 10^{14} ions/ cm^2 . The flux of ions during irradiation was 10^9 ions/ cm^2/s and the sample surface was kept normal to the ion beam direction. Figure 1(a) shows the partitioning of energy loss for each Xe ion into nuclear and electronic stopping power components, as a function of depth in the δ - $\text{Sc}_4\text{Hf}_3\text{O}_{12}$ target material. The integrated energy losses from electronic and nuclear components calculated from their respective stopping powers are 87.5 and 3.4 MeV. It is important to observe in Fig. 1(a) that electronic stopping far exceeds nuclear stopping over nearly the entire range of the Xe ions in the $\text{Sc}_4\text{Hf}_3\text{O}_{12}$ target (at least until the depth of 7.5 μm in the target where the ion implantation occurs).

X-ray powder diffraction measurements were performed on samples irradiated with fluences exceeding 10^{12} ions/ cm^2 , which corresponds to the conditions of a uniformly irradiated surface due to multiple ion-track overlaps. Diffraction measurements were performed using a Bruker D8 Advance diffractometer equipped with a Göbel mirror for $\text{Cu-K}\alpha$ radiation and a NaI scintillation detector. Data collections were performed in a θ - θ geometry performing symmetric step scans of the detector and the x-ray source ($\Delta 2\theta = 0.02^\circ$) with a step time of 2 sec/step. δ - $\text{Sc}_4\text{Hf}_3\text{O}_{12}$ presents a significant advantage for the x-ray diffraction analysis compared to other compounds belonging to this same family because of the excellent scattering contrast between Sc and Hf ions.

Figure 1(b) shows the depth profile of implanted Xe ions in δ - $\text{Sc}_4\text{Hf}_3\text{O}_{12}$, calculated using SRIM [30] for 10^{14} ions/ cm^2 . Based on SRIM, the projected range, R_p , of 92 MeV Xe ions in δ - $\text{Sc}_4\text{Hf}_3\text{O}_{12}$ is 8 μm , with a longitudinal straggling of 0.7 μm . Figure 1(b) also shows the penetration depth of $\text{Cu-K}\alpha$ x-rays in δ - $\text{Sc}_4\text{Hf}_3\text{O}_{12}$. The x-ray diffracted signal in δ - $\text{Sc}_4\text{Hf}_3\text{O}_{12}$ comes from a variable penetration depth not exceeding 5 μm . Clearly, over this range in target depth, no significant Xe ion implantation occurs. In summary, Fig. 1 shows that electronic energy loss dominates significantly over

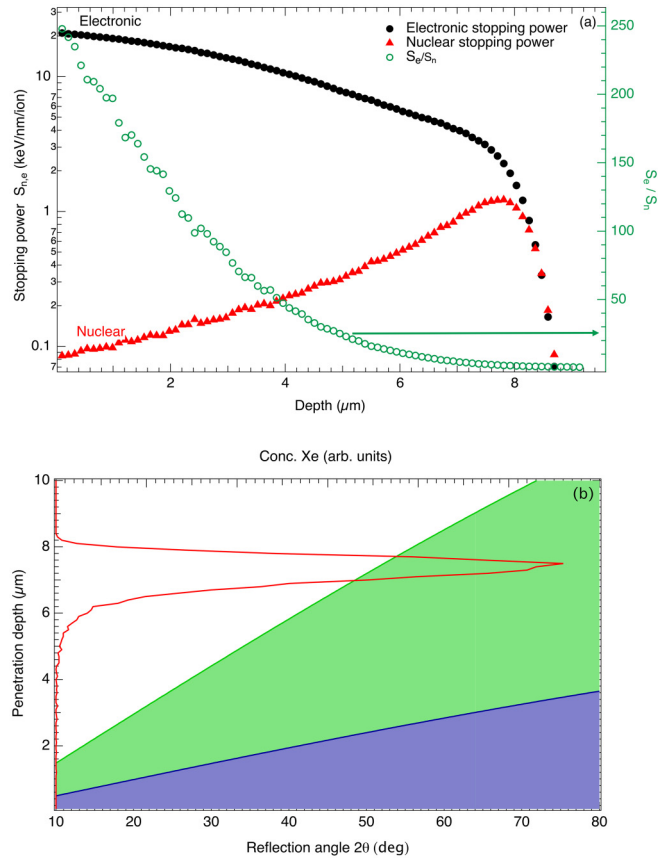


FIG. 1. (a) Electronic versus nuclear energy loss for 92 MeV Xe ions in $\delta\text{-Sc}_4\text{Hf}_3\text{O}_{12}$. The abscissa indicates distance into the target, specifically distance normal to the target surface. The projected (longitudinal) range of the incident Xe ions is approximately 8 μm . The ordinate on the left shows incident ion energy loss [due to either electronic (black circles) or nuclear (ballistic; red triangles) mechanisms] on the logarithmic scale, while that on the left shows the ratio of electronic to nuclear energy loss (green open circles). Calculations were performed using the so-called “quick SRIM” calculations option within the SRIM code for ion stopping in solids [30]. (b) Comparison of the penetration depth of Cu-K α x rays in $\delta\text{-Sc}_4\text{Hf}_3\text{O}_{12}$ as a function of the scattering angle (blue, 2θ , bottom scale) and Xe implantation profile (red line, top scale): according to the Beer-Lambert law and for a Bragg-Brentano experiment geometry, 63.2% of the scattered signal at a given angle comes from a shallow region below the sample surface whose depth is below the blue line. The green line is intended to indicate that 95% of the signal arises from depths below this line. Below $2\theta = 45^\circ$, more than 95% of the scattered x-ray photons come from a region where no implantation occurs.

nuclear energy loss for 92 MeV Xe in $\delta\text{-Sc}_4\text{Hf}_3\text{O}_{12}$, over nearly the entire range of the implanted Xe ions; additionally, x-ray diffraction measurements at low angles ($2\theta < 45$) are only sensitive to electronic radiation damage effects (essentially, no nuclear radiation damage effects contribute to the measurements performed in this study). Rietveld refinements were performed using the software Jana2000 [31] and 3D structure visualization models were obtained using the software VESTA [32].

III. LOCAL ORDER

The interaction of an impinging x-ray beam with a crystal produces a discrete set of scattered beams forming a periodic lattice of sharp reflections (Bragg reflections), the so-called reciprocal space of the crystal. Any kind of crystal imperfection (stacking faults, chemical disorder, lattice vibrations, ...) perturbing the long-range crystalline order reduces the intensity of the Bragg reflections by a large attenuation factor. But the overall scattered intensity is conserved, and this loss of intensity of the Bragg reflections is, however, recovered under the form of a very weak and broad diffuse intensity that adds to the background and it is spread over particular positions in the reciprocal space. This broad x-ray scattering intensity is called diffuse scattering. The deviation from the perfect crystalline order can occur because of atomic displacements or is related to atomic substitutions, or is due to a combination of the two effects. When the diffracted beam is measured without energy resolution, it is not possible to discriminate between a dynamic origin of the diffuse scattering (lattice vibrations) or a static origin (crystal imperfections). In this setup, the diffuse scattering intensity gives directly the instantaneous spatial correlations of the order parameter ξ : $S(\mathbf{q}, t = 0) = |\xi_q|^2$, where ξ_q is the q th component of the Fourier transform of a spatially dependent atomic displacement wave or density concentration wave occurring in the crystal [33–35]. The spatial correlation length of the q th component of the order parameter can be obtained from the breadth of the diffuse scattering within the Ornstein-Zernike formalism [36,37]. Using a correlated microdiffraction model developed by Neder *et al.* [38] it is possible to model the diffuse scattering produced by correlated nanodomains introducing a difference structure where the atoms represent the difference between the average structure and the nanodomain structure. Scherrer-type peak broadening can be included in this “correlated-model” structure, and it describes the characteristic long-range correlation length of the average structure and the shorter-range averaged size of the correlation domains responsible for the diffuse scattering. Eventually, a microstrain-type peak broadening can also be introduced to account for defect-induced elastic fluctuations of the lattice parameter.

IV. PRISTINE $\delta\text{-Sc}_4\text{Hf}_3\text{O}_{12}$

The Rietveld refinement of the pristine diffraction pattern uses the prototype δ -phase model for A_6BO_{12} [17,18] as a starting point. In these structures, the hexavalent metal ion occupies consistently the 3a positions of the $R\bar{3}$ space group. The trivalent metal ions occupy the 18f Wyckoff positions. O vacancies are localized at 6c positions. In $\delta\text{-Sc}_4\text{Hf}_3\text{O}_{12}$, Sc and Hf cannot order in the same way as their relative ratio is different, and they were evenly distributed over each of these two cation sites in such a way as to maintain the 4:3 cation stoichiometry.

The refinement of this initial model against the pristine sample data allows us to check the validity of the assumption that O vacancies are confined to the 6c Wyckoff position. See note I in the Supplemental Material for further explanation [39]. Also, the relative occupancy of Sc and Hf was refined independently for the 3a and 18f Wyckoff positions occupied

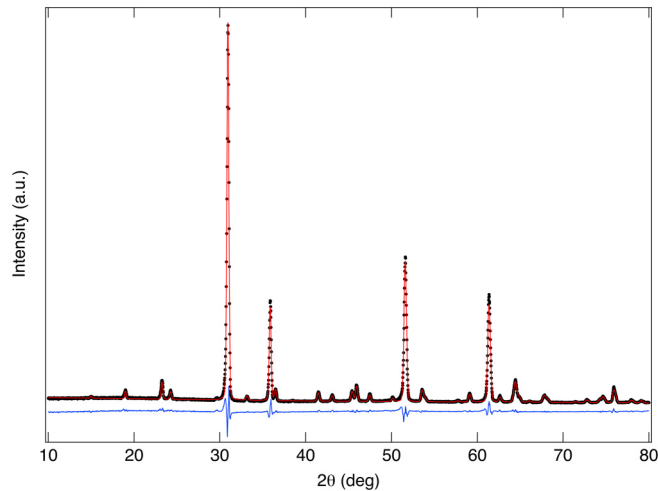


FIG. 2. Observed (black dots) and calculated (red solid line) XRD pattern for pristine δ - $\text{Sc}_4\text{Hf}_3\text{O}_{12}$ showing a good Rietveld refined fit with the structural model shown in Table I. The blue solid line indicates the difference between the observed and calculated patterns.

by cations. The refined and experimental patterns display a very good agreement as displayed in Fig. 2. The refined model provides the calculated stoichiometry of $\text{Sc}_{4.01}\text{Hf}_{2.99}\text{O}_{12}$, in excellent agreement with the desired 4:3:12 stoichiometry. The metal distributions onto the two families of metal sites are not random as initially expected: scandium ions display a mild preference for the 18f sites, while the hafnium ions display a preference for the 3a sites. The refined structural parameters are summarized in Table I. To reduce the overall number of parameters, a common isotropic thermal displacement parameter was used for all the atoms. See note II in the Supplemental Material for details on the model for the profile function used in the refinements [39].

For the purpose of this study we refer to the $A_4^{+3}B_3^{+4}O_{12}$ stoichiometry as the δ phase. The diffraction pattern consists of two types of reflections, strong intense peaks belonging to an average fluorite lattice, and weak superlattice peaks whose intensity depends on the specific ordering of anion vacancies and the corresponding relaxation of the cations from the ideal fluorite positions.

The c/a ratio obtained from the refinement of the pristine δ phase is 0.92837(9), which is more elongated than the corresponding value for an ideal fluorite structure. In addition, the atomic volume for pristine δ - $\text{Sc}_4\text{Hf}_3\text{O}_{12}$ was determined to be $11.5765 \text{ \AA}^3/\text{atom}$.

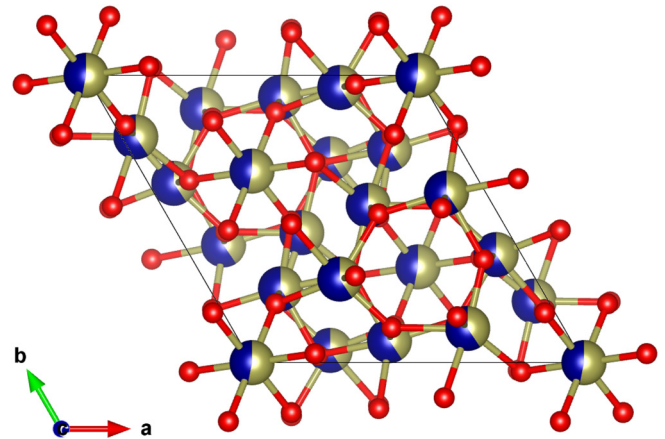


FIG. 3. 3D ball-and-stick structural model of $\text{Sc}_4\text{Hf}_3\text{O}_{12}$ projected along the c axis. The dual colored atoms display cations with a fractional occupancy of Sc (blue) and Hf (gold).

Figure 3 displays a projection of the refined structure showing the occupancy of cations over the 3a and 18f Wyckoff positions and the atomic relaxations. The metal ions at the 3a positions are 6-fold coordinated with the O2 anions forming a regular octahedron with 6 identical metal-oxygen bonds [$2.019(11) \text{ \AA}$]. Here, the environment of the 3a site is very compact as outlined by the large values of the Hf and Sc bond valence sums that are 4.63(7) and 3.79(6), respectively. On the other hand, a distorted polyhedron (capped octahedron) with 7 different bonds ranging from $2.022(16)$ to $2.476(14) \text{ \AA}$ is formed by the cations at the 18f positions with O1 and O2 anions. These bonds are much shorter than what can be expected for Sc and Hf, suggesting that these atoms are actually in an environment much smaller than desirable and more adapted to cations with smaller sizes and/or higher formal valence. It is useful to point out that the longest bond is demonstrably longer than the other six, and it contributes effectively only for 6% to the overall bond valence sum of the cations at 18f positions. This long bond is formed with an O2 atom. For that reason, the cations at 18f positions can be approximately described as a 6-fold-coordinated distorted octahedron. The volume of the polyhedron at 3a is 10.356 \AA^3 while that at 18f is 11.581 \AA^3 (it would be 15.281 \AA^3 , should the longest bond be taken into account in the capped octahedron description). The octahedron at the 3a position has a corner-sharing connectivity with the 6 neighboring 6-fold-coordinated polyhedra of the second type (18f), whereas the 18f polyhedra display an edge-sharing connectivity among themselves in addition to the corner-sharing connectivity already described.

TABLE I. Structural parameters of the refined δ -phase model for $R\bar{3}$, $a = b = 9.3626(4)$, $c = 8.6920(7) \text{ \AA}$, $Z = 3$. $R_{wp} = 9.64\%$, $\text{GoF} = 2.3$, $R_B = 2.4\%$.

	Site	x	y	z	Occ	$U_{\text{iso}} (\text{\AA}^2)$
(Hf, Sc) ₁	3a	0	0	0	0.54(1), 0.46(1)	0.003(1)
(Hf, Sc) ₂	18f	0.2568(2)	0.0426(3)	0.3523(2)	0.409(8), 0.591(8)	0.003(1)
O \square	6c	0	0	1/4	0	
O ₁	18f	0.815(2)	0.789(2)	0.617(2)	1	0.003(1)
O ₂	18f	-0.160(2)	-0.462(2)	0.226(2)	1	0.003(1)

This description is adopted in the rest of this paper. (If the 18f polyhedra were assumed to be 7-fold-coordinated capped octahedra, the connectivity would be exclusively edge sharing for all polyhedra, but the analysis of the volumes of these capped octahedra is quantitatively less convenient, though it leads to the same conclusions). Figure S1 in the Supplemental Material is included to display the conventional building block of δ -Sc₄Hf₃O₁₂ consisting of 7 polyhedra [39].

V. IRRADIATED δ -Sc₄Hf₃O₁₂

Figure 4 shows the measured diffraction patterns of the pristine and irradiated δ -phase samples. A gradual decrease of the superlattice reflections characteristic of the δ phase is observed in the initial stages of the irradiation. These superlattice reflections are also increasingly broadened while the reflections corresponding to a fluorite average structure are only marginally affected by a microstrain effect related to an inhomogeneous defect buildup. This suggests that the characteristic correlation length of the δ phase is continuously reduced as the irradiation proceeds. The underlying mechanism controlling these changes is not clear, but partial healing of the defects can be achieved by the significant atomic transport occurring in the anion sublattice. The corresponding correlation length of the damaged δ phase remains much larger than the transverse dimension of the region impacted by a single ion track as long as these superlattice reflections are observed. Above 6×10^{12} Xe/cm², these superlattice reflections vanish, leaving behind only the parent fluorite peaks and diffuse scattering. This indicates that irradiation-induced defects cause the ordered δ -phase structure to transition to something resembling a defect fluorite phase that still possesses residual short-range order. Rietveld refinements of diffraction patterns up to the fluence of 6×10^{12} Xe/cm² were carried out using the δ -phase model obtained from the pristine sample. The refinement of the pattern at 10^{13} Xe/cm² does not provide the proper feedback for determining the phases of

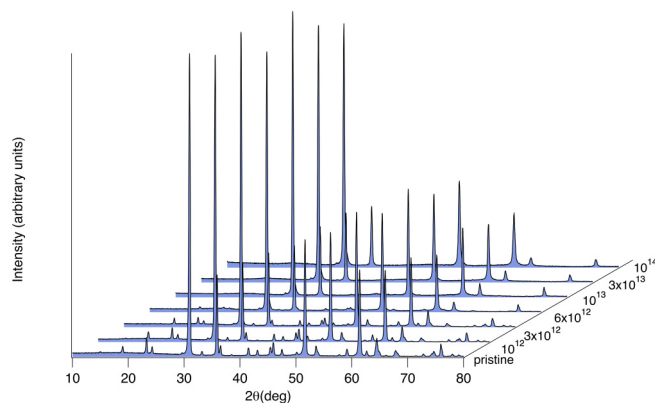


FIG. 4. X-ray diffraction patterns obtained from pristine and 92 MeV Xe irradiated Sc₄Hf₃O₁₂ at fluences ranging from 10¹¹–10¹⁴ Xe/cm². The vanishing of superlattice reflections characteristic of the trigonal δ phase occurs above 6×10^{12} Xe/cm². Before that apparent long-range symmetry changes, the intensity of those superlattice reflections decreases continuously due to a progressive change in the crystal structure.

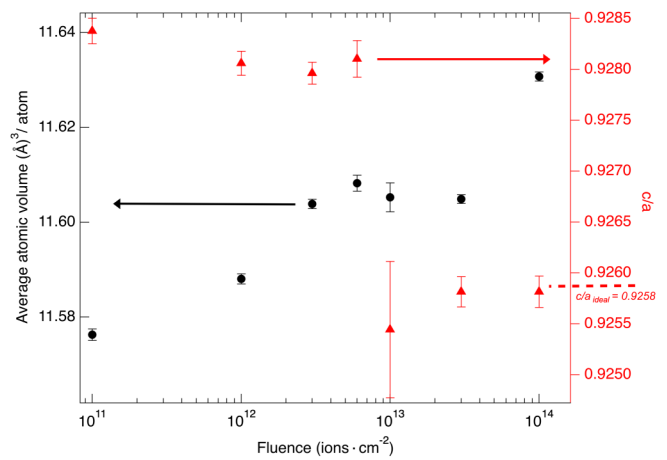


FIG. 5. Changes in the average atomic volume (black circles) and c/a lattice parameter (red triangles) as a function of Xe fluence. The average atomic volume displays a monotonic increase as a function of the fluence, regardless of the symmetry changes. The c/a on the other hand shows an abrupt change above 6×10^{12} ions/cm² marking a change in the long-range symmetry. Ideal c/a for fluorite is shown as dotted line. For comparison purposes, the lattice parameters were always calculated in the trigonal symmetry of the pristine phase, though above 10^{13} ions/cm² the lattice becomes cubic. Note that the c/a ratio and atomic volume for pristine δ -Sc₄Hf₃O₁₂ (not shown here) are 0.92837(9) and 11.5765 Å³/atom, respectively, and are extremely close to those obtained for the sample irradiated with 1×10^{11} ions/cm².

the atomic displacements and this leads to larger thermal displacement parameters in the average fluorite structure. Hence, from here onward, the observed reflections were only refined using a fluorite average structure while the diffuse scattering can be modeled using a correlated microdomain approach.

Ion irradiation in this δ phase produces two different types of observable changes. The first type of modification concerns long-range perturbation of the lattice related to elastic and polar interactions among structural defects. These changes alter the volume of the reference cell and its shape that was characterized by the c/a ratio in this present case. The second type of modification is short-range and affects more directly the relaxation of the atomic structure characterized by composition and relaxation of the atomic positions. It can then also induce polymorphism of the structural motifs and change the polyhedra connectivities, thus building up competition between local configurations.

Changes in the average atomic volume and c/a lattice parameter obtained from these refinements are displayed in Fig. 5. The atomic volume and the a -lattice parameter increase with increasing fluence. At lower fluences, a progressive convergence of c/a toward the ideal fluorite ratio (0.9258) is observed. Then, at 10^{13} Xe/cm², a sudden decrease in the c -lattice parameter occurs, pinning the c/a to the ideal value. This change is concomitant with the disappearance of the superlattice reflections.

On the other hand, the thermal displacement parameter (U_{iso}) displayed in Fig. 6 shows a gradual increase before practically saturating after the transformation to long-range fluorite. This indicates a high degree of displacive disorder in

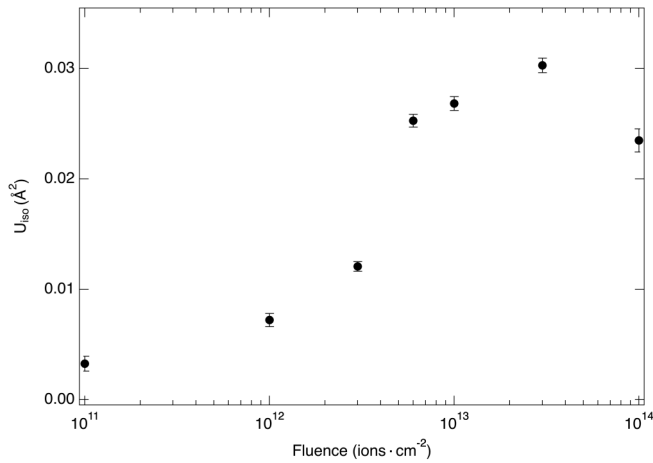


FIG. 6. Thermal displacement parameters (U_{iso}) as a function of fluence for pristine and 92 MeV Xe irradiated $\text{Sc}_4\text{Hf}_3\text{O}_{12}$. U_{iso} parameters were obtained after Rietveld refinement and indicate an increase of disorder in the δ phase which gradually saturates when the structure is transformed to a defect fluorite phase.

the long-range average fluorite structure. The overall atomic displacement parameter $\text{ADP}(U_{\text{iso}})$ is 0.003 \AA^2 for the pristine sample and it increases steadily at higher fluences to saturate around 0.03 \AA^2 . Note III and Fig. S2 in the Supplemental Material are included to display the evolution of $\text{ADP}(U_{\text{iso}})$ as a function of the fluence on a linear scale which shows the value for the pristine sample [39].

The six identical metal to oxygen bond lengths for 3a octahedra (those at the corners of Fig. 3) increase from $2.019(11) \text{ \AA}$ to $2.164(16) \text{ \AA}$ while the average of the 6 shorter bond lengths for the cations at 18f positions decreases from 2.15 \AA to 2.13 \AA . It can be seen that the shared edges among 18f octahedra are shortened after irradiation, which is a result of the swelling of 3a-type octahedra. These modifications to the structural motif cause an overall increase in the distortion of the structure that is not akin to the convergence toward a long-range fluorite as observed for the lattice parameters. At lower fluence, a quantitative evolution of polyhedral volumes can be obtained in the δ -phase structure. A 23% increase in the volume of octahedra around the 3a site is observed between the pristine and the sample irradiated at a fluence of $6 \times 10^{12} \text{ Xe/cm}^2$, whereas a decrease of 10% in the octahedral volume around the 18f site is also observed. The change in volume of these polyhedra at $6 \times 10^{12} \text{ Xe/cm}^2$ converges to the volumes observed in the two bixbyite polyhedra (10.42 and 12.95 \AA^3). Hence, the local and long-range changes are thus divergent and the local structure is not averaging to an ideal fluorite where cation and anion vacancies are distributed at random.

Indeed, at 10^{13} Xe/cm^2 a diffuse scattering signal appears (Fig. 7). The angular positions of the diffuse scattering components of the scattering do not change at fluences above 10^{13} Xe/cm^2 . These positions do not overlap with the positions of the pristine δ -phase superlattice peaks but rather correspond to new positions compatible with superlattice reflections of a bixbyite-type structure. In spite of the O stoichiometry, these positions are not compatible with a pyrochlore structural arrangement because they do not satisfy the F -center

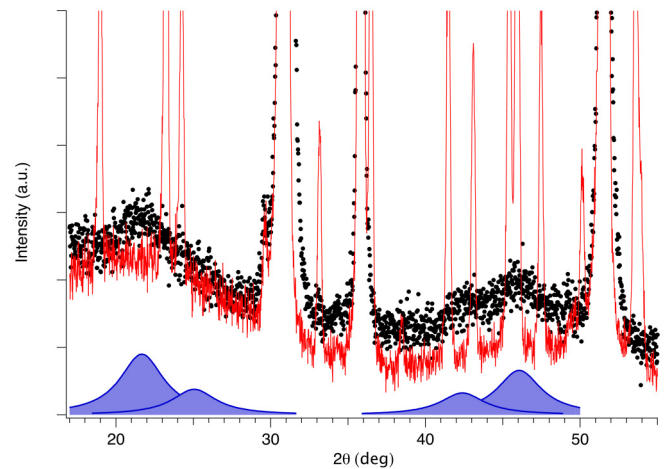


FIG. 7. XRD patterns obtained from $\text{Sc}_4\text{Hf}_3\text{O}_{12}$, pristine delta phase (solid red) and irradiated with 10^{14} Xe/cm^2 (black dots), showing emergence of diffuse scattering (blue peaks) at the angular positions corresponding to (211), (220), (332), and (413) superlattice reflections of bixbyite-related structures ($Ia\bar{3}, a_B = 2a_F$).

extinction rules. Also, the diffuse signal at (211) is not compatible with an $a_W = \sqrt{2}a_F, b_W = 2a_F, c_W = \sqrt{2}a_F$ *Imma* weberite arrangement.

The bixbyite-like arrangement hypothesis is also in agreement with the observation of diffuse spots at the bixbyite reciprocal lattice points by TEM in low-energy irradiation experiments on δ -phase samples [20,21]. While pyrochlore and weberite structures are characterized by a cation site preference onto the A and B sites of the generic $A_2B_2O_7$ chemical formula, in the bixbyite-related structures $M_2O_{3.5}$ a pronounced cation selectivity is not expected and the bixbyite order displayed schematically in Fig. 8 is only given by the stacking of the O vacancies and the atom position relaxation they induce. This particular order might be related to the moderate cation selectivity and the pronounced O-vacancy

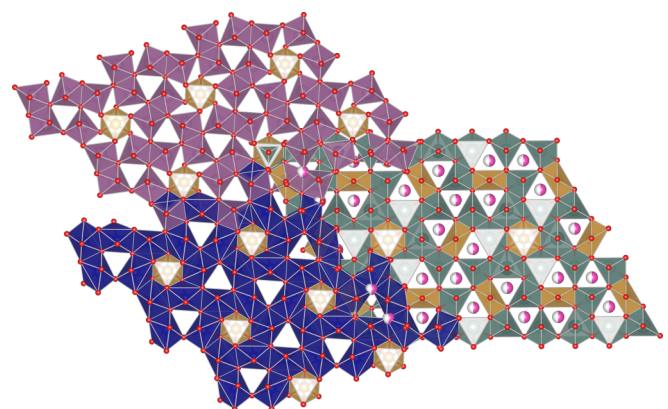


FIG. 8. Schematic changes induced by the ion irradiation on the occupancies of the anion sublattice. The blue and purple structures represent the pristine structure with the two polyhedra descriptions, the green structure on the right the bixbyite-like arrangement where half of the oxygen vacant sites are on average randomly filled (displayed as half-colored pink spheres).

ordering already observed in the pristine δ phase of this compound. The correlation length of this local structure is about 4 nm, as derived from the integral breadth of the diffuse signal. Previously, ion tracks consisting of a disordered fluorite core of 3–4 nm in diameter were reported in swift heavy ion irradiated δ - $\text{Sc}_4\text{Zr}_3\text{O}_{12}$ [22]. The corresponding lattice parameter of the present bixbyite-related local phase is about 9.99(3) Å. Therefore, this phase is almost 2.4% denser than the average long-range radiation-induced oxygen deficient fluorite phase and also 1.9% denser than the pristine δ phase, marking another departure from the evolution in volume of the long-range average-fluorite phase.

We note here that the damage evolution revealed by our XRD measurements is also not compatible with conventional radiation-induced phase transformation models, such as the “Gibbons” cascade overlap models [40,41]. These models require that the latent damage in the cascade regions produce a second phase that is not correlated and generally incoherent with the pristine (unirradiated) material. On the contrary, our latent damage regions are likely coherent with the undamaged regions; evidence for this is provided in TEM images in Tang *et al.* [22], where they observed coherence between latent tracks and pristine material in swift heavy ion irradiated $\text{Sc}_4\text{Zr}_3\text{O}_{12}$ (the oxide structure and irradiation conditions in Tang *et al.* are very similar to the compound and experimental conditions used in this study). Furthermore, were we to have coexisting delta and disordered fluorite phases in our low-fluence microstructures (i.e., fluences ranging from 10^{11} to 6×10^{12} ions/cm²), we should expect to resolve two sets of XRD peaks: one from the rhombohedrally distorted δ phase (c/a greater than ideal); the second from the cubic disordered fluorite phase (with the ideal c/a ratio). We do not observe this hypothetical mixture at any fluence, based on our XRD measurements.

VI. DISCUSSION AND CONCLUSION

According to the previous work of Ishimaru *et al.* [20], low-energy ion irradiation (300 keV Kr and up to a fluence of 3×10^{16} ions/cm²) induces structural changes in the δ -phase compound $\text{Sc}_4\text{Zr}_3\text{O}_{12}$. Using cross-section TEM, two different phases were observed in the sample. These phases occur in two separate layers located above the pristine sample substrate: the diffraction pattern from the layer immediately above the substrate only presented spots characteristic of a fluorite phase, while the layer closer to the surface presented additional diffuse spots obeying the selection rules of the $Ia\bar{3}$ space group. This was then indexed with a bixbyite-type structure. The authors concluded that this phase was likely formed by some sort of rearrangement of oxygen vacancies within the fluorite layer. The existence of the two layers seems related to the characteristics of the low-energy irradiation, where damage occurs in the absence of implanted ions in the

bixbyite-type layer, whereas damage coincides with significant ion implantation in the fluorite-like layer. In the present experiment, no implantation occurs within the layer probed by x rays and indeed, only a disordered fluorite with bixbyite local flavor is observed.

Group-subgroup analysis establishes that there is no direct compatibility relation between bixbyite and the δ phase, thus preventing the existence of an order parameter describing the direct transformation. The only possible pathway to connect the two phases is through an intermediate fluorite phase that shares the specific symmetry elements of bixbyite and the δ phase. Bixbyite and the δ phase share a unique feature among the phases observed in the pseudobinary phase diagrams of type $A_2^{+3}O_3$ – $B^{+4}O_2$: these two phases are the only ones where the metal ions are 6-fold coordinated with O anions.

The δ phase can also be viewed as having capped octahedra which are found in the A-type M_2O_3 compounds. A known high-temperature phase transformation occurs from the A-type into a C-type bixbyite in some of these rare-earth oxides. Hence it is possible to change from 7-fold to 6-fold in these sesquioxides and the same is likely to occur in the δ structure. Therefore, it is likely that these two phases actually exhibit some sort of competition. Though the two phases have qualitatively similar polyhedra, they do not have exactly the same connectivity, and this explains the different O stoichiometries.

The bixbyite phase generally presents an extended domain of existence in the oxygen-excess range, as for instance in CeO_{2-x} , TbO_{2-x} , and PrO_{2-x} [42,43] ($0.28 \leq x \leq 0.5$). Thus, the bixbyite signature from a structure with extra O atoms filling the bixbyite O vacancies would translate into weak superstructure peaks, similar to the diffuse scattering observed, as the amplitudes of the cation relaxations near the O vacancies would be smaller. This observation suggests that the bixbyite phase acts possibly as a chemical attractor, having some kind of exotic dynamics for local chaotic fluctuations of the oxygen stoichiometry. The bixbyite local configuration reached after ion irradiation is then a frozen metastable steady state where the phase trajectories evolving away from the δ -phase composition remain in the vicinity of the bixbyite attractor. This particular characteristic of the bixbyite phase seems effective in supporting radiation tolerance, by creating a very large number of frozen local configurations of lower symmetry—preserving a very large number of configurations that maximize and thereby stabilize the apparent long-range cubic symmetry. Systems exhibiting these characteristics can then be exploited to effectively engineer radiation-resistant materials.

ACKNOWLEDGMENT

The authors would like to acknowledge Dr. Isabelle Monnet and Dr. Jean-Claude Pivin for their help in performing the ion irradiation experiment at GANIL.

[1] C. Wagner and W. Schottky, Theorie der geordneten mischphasen, *Z. Physikal. Chem. B* **11**, 163 (1930).

[2] O. T. Sørensen, *Nonstoichiometric Oxides* (Academic Press, 1981).

- [3] L. Cai and J. C. Nino. Complex ceramic structures. I. Weberites, *Acta Crystallogr., Sect. B: Struct. Sci.* **65**, 269 (2009).
- [4] K. E. Sickafus, L. Minervini, R. W. Grimes, J. A. Valdez, M. Ishimaru, F. Li, K. J. McClellan, and T. Hartmann, Radiation tolerance of complex oxides, *Science* **289**, 748 (2000).
- [5] B. J. Wuensch and K. W. Eberman, Order-disorder phenomena in $A_2B_2O_7$ pyrochlore oxides, *JOM* **52**, 19 (2000).
- [6] M. Lang *et al.*, Review of $A_2B_2O_7$ pyrochlore response to irradiation and pressure, *Nucl. Instrum. Methods Phys. Res., Sect. B* **268**, 2951 (2010).
- [7] Y. H. Li, B. P. Uberuaga, C. Jiang, S. Choudhury, J. A. Valdez, M. K. Patel, J. Won, Y.-Q. Wang, M. Tang, D. J. Safarik, D. D. Byler, K. J. McClellan, I. O. Usov, T. Hartmann, G. Baldinozzi, and K. E. Sickafus, Role of Antisite Disorder on Preamorphization Swelling in Titanate Pyrochlores, *Phys. Rev. Lett.* **108**, 195504 (2012).
- [8] J. Shamblin, M. Feyngenson, J. Neufeind, C. L. Tracy, F. Zhang, S. Finkeldei, D. Bosbach, H. Zhou, R. C. Ewing, and M. Lang, Probing disorder in isometric pyrochlore and related complex oxides, *Nat. Mater.* **15**, 507 (2016).
- [9] D. Simeone, G. J. Thorogood, D. Huo *et al.*, Intricate disorder in defect fluorite/pyrochlore: A concord of chemistry and crystallography, *Sci. Rep.* **7**, 3727 (2017).
- [10] G. Pilania, B. Puchala, and B. Uberuaga, Distortion-stabilized ordered structures in $A_2BB'O_7$ mixed pyrochlores, *npj Comput. Mater.* **5**, 7 (2019).
- [11] M. Tang, J. A. Valdez, K. E. Sickafus, and P. Lu, Order-disorder phase transformation in ion-irradiated rare earth sesquioxides, *Appl. Phys. Lett.* **90**, 151907 (2007).
- [12] C. L. Tracy, M. Lang, F. Zhang, C. Trautmann, and R. C. Ewing, Phase transformations in Ln_2O_3 materials irradiated with swift heavy ions, *Phys. Rev. B* **92**, 174101 (2015).
- [13] G. Sattonnay, S. Bilgen, L. Thome, C. Grygiel, I. Monnet, O. Plantevin, C. Huet, S. Miro, and P. Simon, Structural and microstructural tailoring of rare earth sesquioxides by swift heavy ion irradiation, *Phys. Status Solidi B* **253**, 2110 (2016).
- [14] G. Baldinozzi, J.-F. Berar, M. Gautier-Soyer, and G. Calvarin, Segregation and site selectivity in Zr-doped Y_2O_3 , *J. Phys.: Condens. Matter* **9**, 9731 (1997).
- [15] G. Baldinozzi, J.-F. Berar, and G. Calvarin, Rietveld refinement of two-phase Zr-doped Y_2O_3 , *Mater. Sci. Forum* **278**, 680 (1998).
- [16] H. J. Rossell, Crystal structures of some fluorite-related M_7O_{12} compounds, *J. Solid State Chem.* **19**, 103 (1976).
- [17] Y. Hinatsu, N. Masaki, and T. Fujino, The crystal structure of La_6UO_{12} , *J. Solid State Chem.* **73**, 567 (1988).
- [18] R. M. Rojas, P. Herrero, P. J. Garcia Chain, and J. Rodriguez-Carvajal, Structural study of the rhombohedral fluorite-related R_{III} phase $U_{1-y}La_yO_{2\pm x}$, $0.56 \leq y \leq 0.67$, *J. Solid State Chem.* **112**, 322 (1994).
- [19] J. A. Valdez, M. Tang, and K. E. Sickafus, Radiation damage effects in δ - $Sc_4Zr_3O_{12}$ irradiated with Kr^{2+} ions under cryogenic conditions, *Nucl. Instrum. Methods Phys. Res., Sect. B* **250**, 148 (2006).
- [20] M. Ishimaru, Y. Hirotsu, M. Tang, J. A. Valdez, and K. E. Sickafus, Ion-beam-induced phase transformations in δ - $Sc_4Zr_3O_{12}$, *J. Appl. Phys.* **102**, 063532 (2007).
- [21] K. E. Sickafus, M. Ishimaru, Y. Hirotsu, I. Usov, J. A. Valdez, P. Hosemann, A. L. Johnson, and T. T. Thao, Compositional analyses of ion-irradiation-induced phases in δ - $Sc_4Zr_3O_{12}$, *Nucl. Instrum. Methods Phys. Res., Sect. B* **266**, 2892 (2008).
- [22] M. Tang, P. Kluth, J. Zhang, M. K. Patel, B. P. Uberuaga, C. J. Olson Reichhardt, and K. E. Sickafus, Swift heavy ion irradiation-induced microstructure modification of two delta-phase oxides: $Sc_4Zr_3O_{12}$ and $Lu_4Zr_3O_{12}$, *Nucl. Instrum. Methods Phys. Res., Sect. B* **268**, 3243 (2010).
- [23] J. Zhang, Y. Wang, M. Tang, J. Won, J. A. Valdez, and K. E. Sickafus, Order-to-disorder transformation in δ -phase $Sc_4Zr_3O_{12}$ induced by light ion irradiation, *J. Mater. Res.* **25**, 248 (2010).
- [24] J. Wen, C. Gao, Y. H. Li, Y. Q. Wang, L. M. Zhang, B. T. Hu, L. J. Chen, and X. Su, Ion irradiation induced order-to-disorder transformation in δ -phase $Lu_4Hf_3O_{12}$, *Nucl. Instrum. Methods Phys. Res., Sect. B* **310**, 1 (2013).
- [25] J. Wen, Y. H. Li, M. Tang, J. A. Valdez, Y. Q. Wang, M. K. Patel, and K. E. Sickafus, Heavy and light ion irradiation damage effects in δ -phase $Sc_4Hf_3O_{12}$, *Nucl. Instrum. Methods Phys. Res., Sect. B* **365**, 325 (2015).
- [26] J. Zhang, M. K. Patel, Y. Q. Wang, M. Tang, J. Won, J. A. Valdez, and K. E. Sickafus, Strong irradiation tolerance to amorphization in delta- $Sc_4Ti_3O_{12}$, *J. Nucl. Mater.* **459**, 265 (2015).
- [27] B. H. O'Connor and T. M. Valentine, A neutron diffraction study of the crystal structure of the C-form of yttrium sesquioxide, *Acta Crystallogr., Sect. B: Struct. Sci.* **25**, 2140 (1969).
- [28] M. R. Thornber, D. J. M. Bevan, and J. Graham, Mixed oxides of the type MO_2 (fluorite)- M_2O_3 . III. Crystal structures of the intermediate phases $Zr_5Sc_2O_{13}$ and $Zr_4Sc_3O_{12}$, *Acta Crystallogr., Sect. B: Struct. Sci.* **24**, 1183 (1968).
- [29] G. A. Kalinovskaya, F. M. Spiridonov, and L. N. Komissarova, Phase equilibria in the HfO_2 - Sc_2O_3 , *J. Less-Common Metals* **17**, 151 (1969).
- [30] J. F. Ziegler and J. P. Biersack, *The Stopping and Range of Ions in Matter*, Vol. 2–6 (Pergamon Press, New York, 1977).
- [31] V. Petricek, M. Dusek, and L. J. F. Palatinus, Crystallographic computing system JANA2006: General features, *Z. Kristallogr.* **229**, 345 (2014).
- [32] K. Momma and F. Izumi, VESTA 3 for three-dimensional visualization of crystal, volumetric and morphology data, *J. Appl. Cryst.* **44**, 1272 (2011).
- [33] E. Rosshirt, F. Frey, H. Boysen, and H. Jagodzinski, Chain ordering in $E_2PI_{1,6}$ (5, 10-diethylphenazinium iodide), *Acta Crystallogr., Sect. B: Struct. Sci.* **41**, 66 (1985).
- [34] R. J. Nelmes, D. R. Allan, M. I. McMahon, and S. A. Belmonte, Self-Hosting Incommensurate Structure of Barium IV, *Phys. Rev. Lett.* **83**, 4081 (1999).
- [35] T. R. Welberry and B. D. Butler, Interpretation of diffuse x-ray scattering via models of disorder, *J. Appl. Cryst.* **27**, 205 (1994).
- [36] H. Jagodzinski and F. Frey, Disorder diffuse scattering of x-rays and neutrons, *International Tables for Crystallography, Vol. B, Reciprocal Space*, edited by U. Shmueli (Springer, Dordrecht, 2006), pp. 407–442.
- [37] J. Brunet and K. E. Gubbins, General theory of the long-range pair-correlation function, *J. Chem. Phys.* **49**, 5265 (1968).
- [38] R. B. Neder, F. Frey, and H. Schulz, Diffraction theory for diffuse scattering by correlated microdomains in materials with several atoms per unit cell, *Acta Crystallogr., Sect. A* **46**, 792 (1990).

- [39] See Supplemental Material at <http://link.aps.org/supplemental/10.1103/PhysRevMaterials.4.093605> for note I on occupancy of vacant 6c site; note II on profile function model; Fig. S1, which shows the polyhedral model for δ phase; and note III on atomic displacement parameter, as well as Fig. S2.
- [40] J. F. Gibbons, Ion implantation in semiconductors. Part I. Range distribution theory and experiments, *Proc. IEEE* **56**, 295 (1968).
- [41] J. F. Gibbons, Ion implantation in semiconductors. Part II. Damage production and annealing, *Proc. IEEE* **60**, 1062 (1972).
- [42] J. W. McMurray, Thermodynamic assessment of the Pr-O system, *J. Am. Ceram. Soc.* **99**, 1092 (2016).
- [43] B. G. Hyde, D. J. M. Bevan, and L. Eyring, On the praseodymium oxygen system, *Philos. Trans. R. Soc. London A* **259**, 583 (1966).